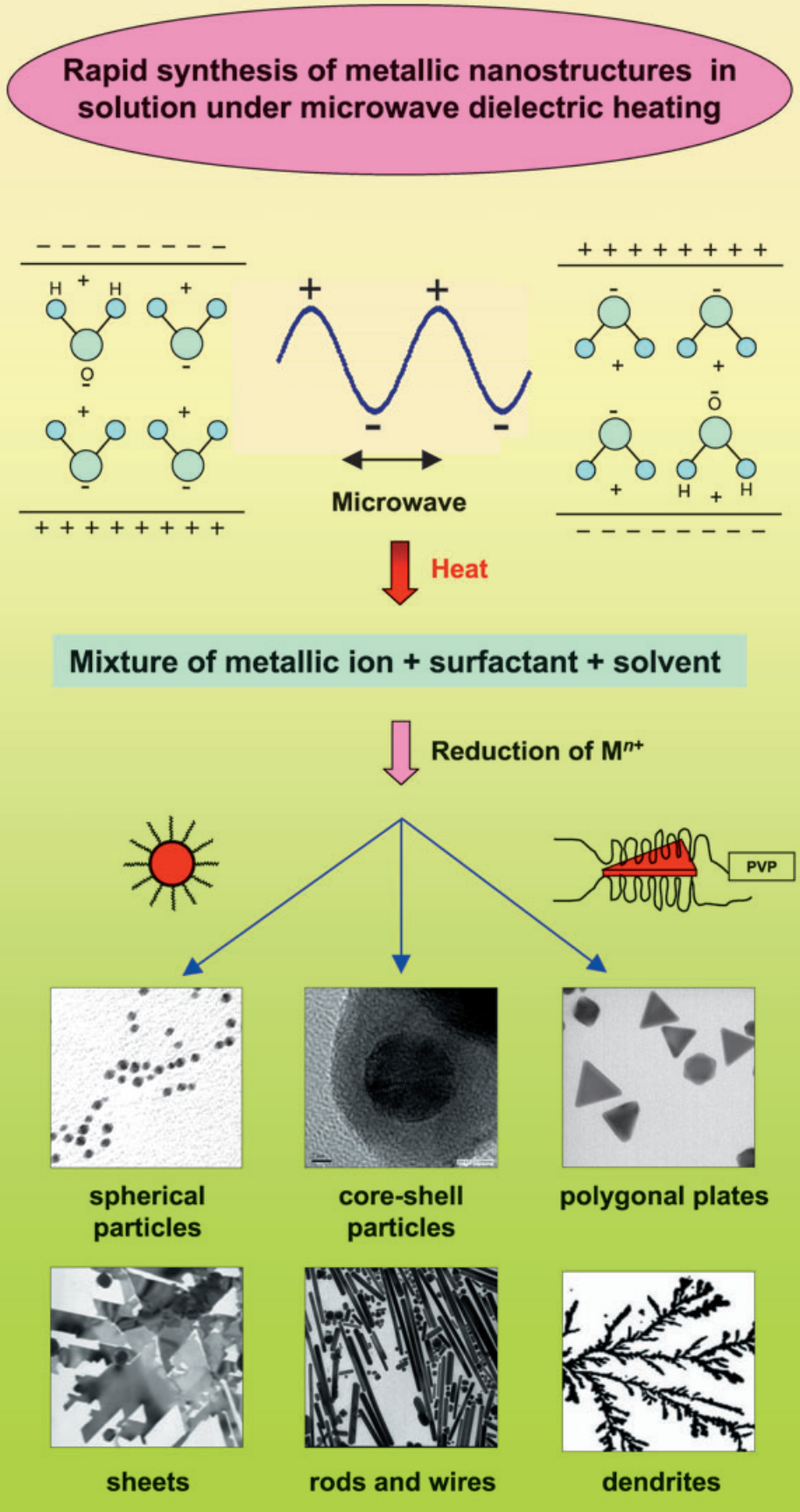

DOI: 10.1002/chem.200400417 *Chem. Eur. J.* **2005**, *11*, 440 – 452

Microwave-Assisted Synthesis of Metallic Nanostructures in Solution

Masaharu Tsuji,*[a] Masayuki Hashimoto,[b] Yuki Nishizawa,[b] Masatoshi Kubokawa,[b] and Takeshi Tsuji[a]

Abstract: Microwave (MW) rapid heating has received considerable attention as a new promising method for the one-pot synthesis of metallic nanostructures in solutions. In this concept, advantageous application of this method has been demonstrated by using some typical examples for the preparation of Ag, Au, Pt, and AuPd nanostructures. Not only spherical nanoparticles, but also single crystalline polygonal plates, sheets, rods, wires, tubes, and dendrites were prepared within a few minutes under MW heating. Morphologies and sizes of nanostructures could be controlled by changing various experimental parameters, such as the concentration of metallic salt and surfactant polymer, the chain length of the surfactant polymer, the solvent, and the reaction temperature. In general, nanostructures with smaller sizes, narrower size distributions, and a higher degree of crystallization were obtained under MW heating than those in conventional oil-bath heating. The origin of these characteristic features under MW irradiation is discussed in terms of thermal and non-thermal effects under MW irradiation.

Keywords: electron diffraction · microwave heating · nanostructures · scanning probe microscopy · thermal effects

[a] Prof. M. Tsuji, Dr. T. Tsuji
Institute for Materials Chemistry and Engineering
Kyushu University, and CREST, Japanese Science and Technology
Kasuga, Fukuoka 816–8580 (Japan)
Fax: (+81) 92-583-7815
E-mail: tsuji@cm.kyushu-u.ac.jp

[b] M. Hashimoto, Y. Nishizawa, M. Kubokawa
Department of Applied Science for Electronics and Materials
Graduate School of Engineering Sciences, Kyushu University
Kasuga, Fukuoka 816–8580 (Japan)

Introduction

A variety of metallic nanostructures, including spherical particles, sheets, plates, rods, wires, tubes, and dendrites have generated significant scientific and technological interest, because of their unique optical as well as novel chemical and catalytic properties. Here, we define nanosheets as thin nanoplates with thickness less than about 10 nm, and nanorods and nanowires as materials with aspect ratios of 2–20 and >20, respectively. These nanostructures have been synthesized by various techniques, including chemical reduction of metallic ions in aqueous or organic solvents.[1–3] In general, chemical reduction has been carried out by heating reagent solutions at 65–200 °C in an oil bath. In the oil-bath heating, the solvent is heated by conduction and convection, so that there is a large temperature distribution within the solvent.

Recently, microwave (MW) dielectric heating has been applied to the rapid synthesis of metallic nanostructures.[4–31] MWs are a portion of the electromagnetic spectrum with frequencies in the range of 300 MHz to 300 GHz. The commonly used frequency is 2.45 GHz. The principle of MW heating of polar molecules is shown in Scheme 1 for the case of H_2O. In the microwave frequency range, polar molecules such as H_2O try to orientate with the electric field. When dipolar molecules try to re-orientate with respect to an alternating electric field, they lose energy in the form of heat by molecular friction.

The MW power dissipation per unit volume in a material (P) is given by Equation (1)]

$$P = c|E|^2 f\varepsilon'' = c|E|^2 f\varepsilon' \tan\delta \quad (1)$$

Here, c is a constant, E is an electric field in the material, f is frequency of radiation, and ε' and ε'' are the dielectric and dielectric loss constants, respectively. ε' represents the relative permittivity, which is a measure of the ability of a molecule to be polarized by an electric field and $\tan\delta = \varepsilon''/\varepsilon'$ is the energy dissipation factor or loss tangent. Equation (1) indicates that ε'' is the most important physical parameter

 DOI: 10.1002/chem.200400417

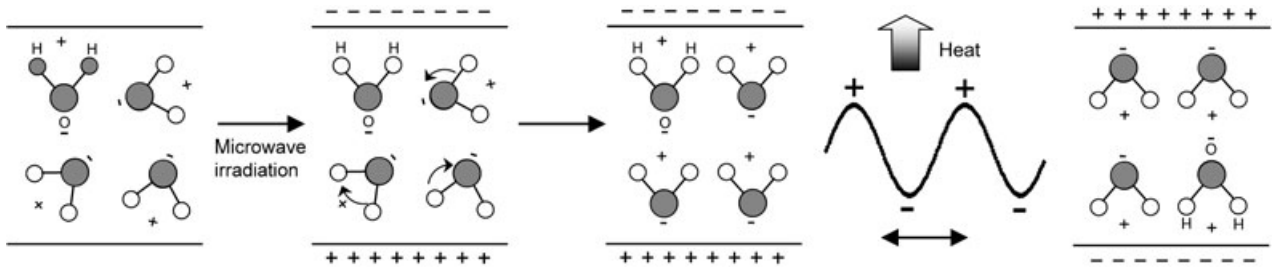

Scheme 1. Heating mechanism of H_2O by microwave irradiation.

that describes the ability of a material to heat in the MW field. The physical parameters of typical solvents used in MW heating for synthesis of metallic nanostructures are listed in Table 1.

Table 1. Physical parameters of typical solvents used for microwave heating.[32]

	B.p. [°C]	ε'	ε''	$\tan\delta$
water	100	78.3	12.3	0.157
methanol	65	32.7	20.9	0.639
ethanol	78	24.3	6.08	0.200
N,*N*-dimethyl formamide (DMF)	153	36.71	–	–
ethylene glycol (EG)	198	41.0	41.0	1.00
N-methyl pyrrolidone (NMP)	202	32.0	8.855	0.277

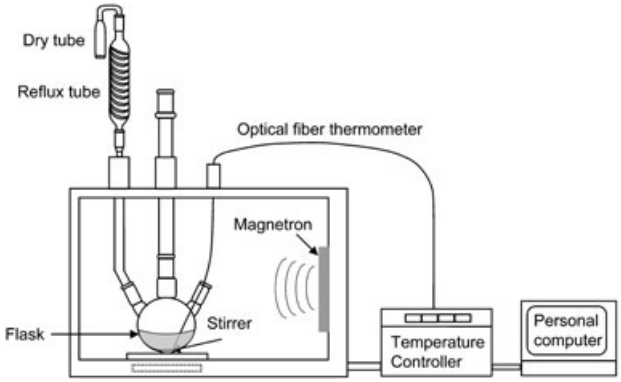

Figure 1. Apparatus used for the microwave-assisted synthesis of metallic nanostructures.

Water, alcohols, DMF, and ethyleneglycol (EG) have high dielectric losses and a high reduction ability. Therefore, they are ideal solvents for MW rapid heating. The MW heating in these solvents in the presence of surfactants has been used to synthesize nanoparticles of various metals (Ni, Ru, Rh, Pd, Ag, Ir, Pt, Au,),[4–23] metallic compounds (PtRu, TiO_2, CdS, CdSe, $MoSe_2$, PbS, HgS, $CuInTe_2$, $CuInSe_2$), and Au/Pd core-shell structures.[24–31] Herein, we focus on recent developments in the areas of MW-assisted synthesis of metallic nanostructures in solutions.

Microwave-Heating Apparatus

A typical experimental apparatus used for the MW heating is shown in Figure 1. A commercial MW oven is modified by installing a condenser and thermocouple through holes in the top and a magnetic stirrer plate coated with Teflon in the bottom of the oven. A thermocouple made of an optical fiber, which is not damaged under MW irradiation, is used. A glass flask is placed in the MW oven with a power of 300–1100 W and connected to a condenser, into which a mixture of metallic salt, surfactant, and, if necessary, a small amount of nucleation reagent is added. A surfactant such as polyvinylpyrrolidone (PVP) acts as a stabilizer for the product nanostructures. The reagent solution is irradiated by MW in a continuous wave (CW) mode or a pulse mode. The pulse mode is more useful for the temperature control of the heating media. Products particles are generally characterized by using transmission electron microscopy (TEM), scanning electron microscopy (SEM), selected area electron diffraction (SAED) pattern, X-ray diffraction (XRD), and UV-visible absorption spectroscopy. Before measuring the TEM photographs, surfactants were often separated from nanostructures by centrifugation.

Possible Effects of MW Heating

There are two kinds of effects of MW dielectric heating: thermal and non-thermal.[33] Thermal effects arise from different temperature regimes under MW heating, whereas non-thermal effects result from effects inherent to the MWs. These effects lead to different morphologies and sizes of metallic nanostructures under MW heating from those in the conventional oil-bath heating.

Thermal effects (effects of rapid and uniform heating): MW provides rapid and uniform heating of reagents, solvents, intermediates, and products. Fast heating accelerates the reduction of metal precursors and the nucleation of the metal cluster, resulting in monodispersed small nanostructures. When MWs are incident perpendicular to the surface of a solvent, their intensity is attenuated in the direction of incidence. However, for the most materials, the distance in the direction of penetration at which the incident power is reduced to half of its initial value is quite long. Therefore, the power dissipation is fairly uniform throughout the solvent.

This homogeneous MW heating also provides uniform nucleation and growth conditions, leading to uniform nanomaterials with small sizes. Due to rapid and homogeneous MW heating, a better crystallinity can be obtained. Therefore, such single-crystalline nanostructures as polygonal plates, rods, and wires could be synthesized efficiently in many cases.

Effects of hot spots and hot surfaces: When some solids heated by MW are involved in the reaction system, hot spots are created on the solid–liquid surfaces. Hot surfaces on solid metals are also created by adsorption of surfactant with a large dielectric loss constant. For example, an aprotic polar molecule *N*-methylpyrrolidone (NMP) has a large dielectric loss constant as shown in Table 1. MW irradiation accelerates the coherent heating of poly(vinyl pyrrolidone) (PVP) as a polymer of NMP and PVP-stabilized metal surfaces. Thus, hot spots will be created on the surfaces stabilized by a surfactant. The uniform formation of hot spots and hot surfaces also accelerate the reduction of metal precursors and the nucleation of the metal cluster, leading to uniform nanostructures with small sizes.

Superheating: Superheating of solvents over boiling points of solvent often occurs as a consequence of the MW dissipation over the whole liquid volume.[32] This effect is especially significant in the presence of a large amount of ions.

Non-thermal effects: In this concept, we define non-thermal effects as those that occur under the same temperature profiles of solvent between MW and oil-bath heating during the reaction. Formation of hot spots and hot surfaces are typical non-thermal effects for the preparation of metallic nanostructures.

MW heating induces various thermal and non-thermal effects described above. In the next section we would like to show some examples of advantageous application of MW heating to the synthesis of metallic nanostructures in solution.

Synthesis of Gold Nanostructures

Preparation of Au spherical nanoparticles: Au nanoparticles have been synthesized by reduction of Au salts in various solvents under oil-bath heating for many hours. When $HAuCl_4$ was reduced in methanol,[5] ethanol,[6] or DMF[8] for 0.5–5 min in the presence of PVP under MW heating (480–1100 W), monodispersed, small spherical nanoparticles, with diameters below 11 nm, were synthesized within a few minutes. Recently, Liu et al.[12] prepared spherical Au particles by using a closed chamber of an MW system with precise temperature control function. When $HAuCl_4$ was reduced in an aqueous solution containing citrate as a stabilizer for 15–30 min, Au particles sizes could be reduced from 85 to 13 nm with increasing reaction temperature, heating time, and rate of temperature increase.

Preparation of Au polygonal plates: We have succeeded in preparation of triangular, truncated-triangular, square, pentagonal, and hexagonal nanoplates by reducing $HAuCl_4$ in EG in the presence of PVP at 198 °C within a few minutes.[13,22] To examine whether the formation of these polygonal nanoplates arises from thermal or non-thermal effects, Au nanostructures obtained under MW heating and oil-bath heating have been compared. Figure 2 shows temperature profiles of the $HAuCl_4$/PVP/EG solution for different heating times with continuous wave (CW) or pulse mode MW irradiation and in an oil-bath. For the solution irradiated by CW MW (400 W), the temperature increases linearly with a fast heating rate and reached 196 °C after 1 min. For the same solution heated in the oil bath (500 W), the temperature increases more slowly. The solution needed 18 min heating in the oil-bath to reach 196 °C. Then, it was kept at the same temperature for 1 min. Thus, the total heating times in MW and oil-bath heating were 2 and 19 min, respectively. A pulse mode of MW was also used, as shown in Figure 2, in order to obtain a similar slow heating rate to that in oil bath.

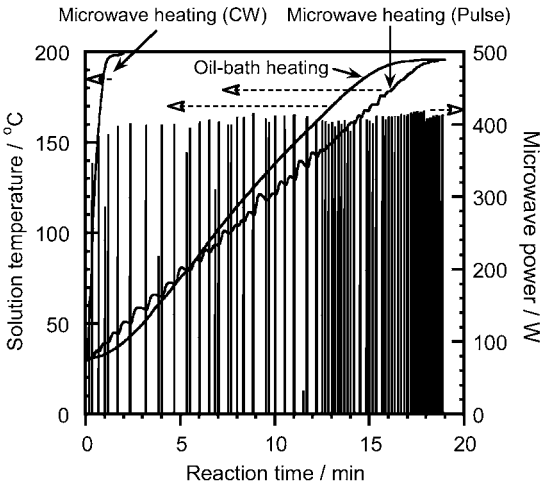

Figure 2. Dependence of temperature on the reaction time for $HAuCl_4 \cdot 4H_2O$/PVP(40 K)/EG heated by CW or pulse MW and in an oil bath. MW pulses used are also shown. Reprinted from reference [13] copyright (2004), with permission from Chemical Society of Japan.

The TEM photographs of Au nanoparticles obtained by CW MW and oil-bath heating as well as histograms of product distributions are compared in Figure 3a and b. It should be noted that besides a small amount of spherical nanoparticles, triangular, square, pentagonal, and hexagonal nanoplates with diameters or edge lengths of 30–90 nm are produced under CW MW irradiation. The uniform contrast of polygonal structures in TEM images clearly demonstrates that these structures are thin plates. In the oil-bath heating, the fraction of large spherical particles (100–190 nm) increases and a small amount of rodlike particles are also formed. Polygonal nanoplates obtained in the oil-bath heat-

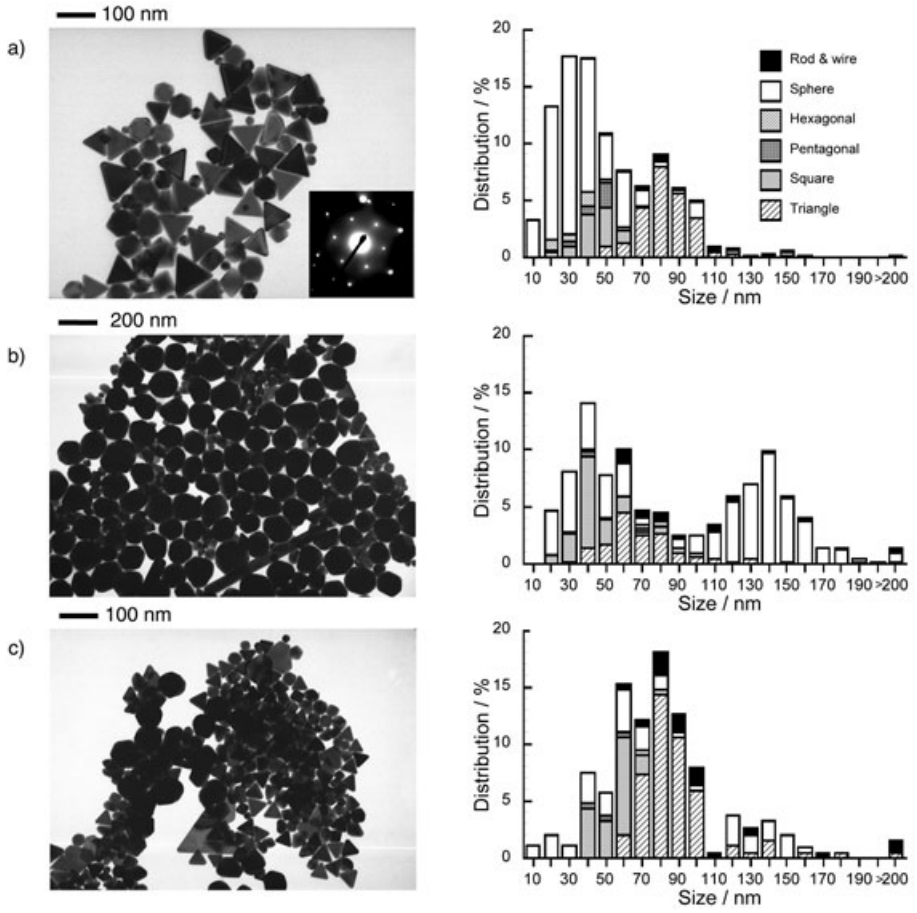

Figure 3. TEM photographs of Au nanostructures obtained by a) CW MW heating for 2 min, b) oil-bath heating for 19 min, and c) pulse MW heating for 19 min, and histograms of product distributions for experiment. Concentrations of $HAuCl_4 \cdot 4H_2O$ and PVP (40 K) were 2.4 mM and 0.25 M, respectively.

ing have less sharp edges than those formed under CW MW heating due to a lower degree of crystallization.

SAED patterns of triangular and hexagonal nanoplates gave the hexagonal symmetry, as shown in Figure 3a. It is therefore rationalized that polygonal nanoplates are single crystals and the incident electron beams are perpendicular to the {111} facets of these nanoplates. The surface free-energy of cubic crystal is in the order of $\gamma_{\{110\}} > \gamma_{\{100\}} > \gamma_{\{111\}}$.[34] Thus, anisotropic growth occurs by uniform heating under MW irradiation, giving the most stable {111} face on the top surface of the nanostructures.

Figure 3c shows the TEM photograph of products formed under pulse MW heating and the product histogram. When the product distribution in pulse MW heating for 19 min was compared with that for the short CW MW heating, the fraction of small spherical particles below 70 nm decreases, while that of large spherical particles in the 120–160 nm region increases. Moreover, the fractions of triangular nanoplates and nanorods increase. These facts indicate that morphologies and sizes of Au nanostructures change by the variation of irradiation conditions such as a CW or pulse mode, heating rate, and heating time.

There are marked differences in the product histograms between pulse MW and oil-bath heating for 19 min. In the case of pulse MW heating, the fraction of triangular nanoplates in the 60–100 nm region is larger, while that of large spherical particles in the 100–200 nm region is smaller than those in the oil-bath heating. The preferential formation of nanoplates under MW heating even at a slow heating rate suggests that non-thermal effects play a significant role. One reason for a higher degree of crystallization leading to single-crystalline Au nanoplates under MW heating must be bursting nucleation due to rapid and homogeneous dielectric heating, which cannot be achieved by oil-bath heating. The other reason will be the formation of hot surface by adsorption of surfancant PVP with a large dielectric loss constant.

Experimental parameters for the control of morphologies and sizes of Au nanoplates: An outstanding feature of MW heating for the preparation of Au nanostructures is the preferential formation of polygonal nanoplates. To control morphologies and sizes of Au nanoplates prepared by MW heating, effects of some selected experimental parameters have been examined.

Effects of the concentrations of $HAuCl_4$ and PVP: Figure 4 shows TEM photographs of Au nanostructures obtained at four typical $HAuCl_4$ and PVP concentrations. It should be noted that morphologies and sizes of Au nanostructures strongly depend on the concentrations of $HAuCl_4$ and PVP. Without addition of PVP, only large spherical gold particles with diameters of 100–300 nm are produced due to fast growth of particles (Figure 4a). This implies that PVP is necessary for the formation of anisotropic polygonal plates, rods, and wires. A mixture of triangular, square, and hexagonal polygonal nanoplates is mainly produced at low $HAuCl_4$ and PVP concentrations (Figure 4b). Small square nanoparticles are preferentially produced at a low concentration of $HAuCl_4$ and a high PVP concentration (Figure 4c), while large triangular and hexagonal plates are preferentially formed at high $HAuCl_4$ and PVP concentrations (Figure 4d). These results indicate that the sizes of particles and plates

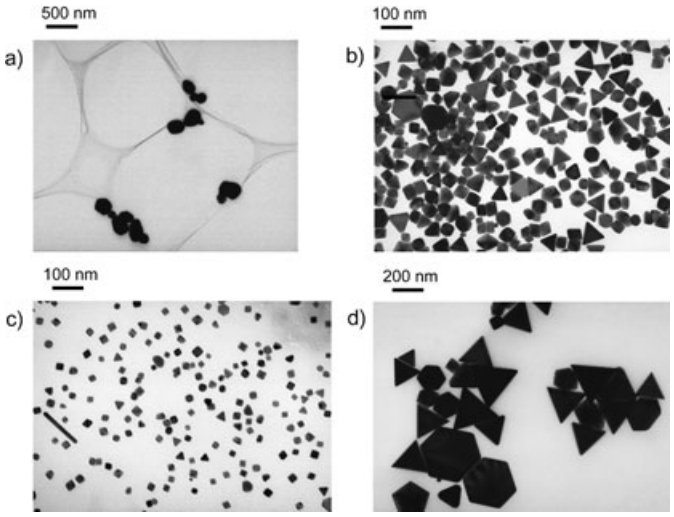

Figure 4. TEM photographs of Au nanostructures obtained by CW MW heating a) for 2 min from $HAuCl_4 \cdot 4H_2O$/EG, b)–d) for 2 min from $HAuCl_4 \cdot 4H_2O$/PVP(40 K)/EG. Concentrations of $HAuCl_4 \cdot 4H_2O$ and PVP were a) 2.4 mM and 0 M, b) 1.2 mM and 0.5 M, c) 2.4 mM and 3 M, and d) 19.2 mM and 2 M, respectively.

generally increase with decreasing the PVP/$HAuCl_4$ molar ratio.

Effects of the chain length of PVP: In Figure 5 TEM photographs of Au nanostructures, the color of their solutions, and the UV-visible absorption spectra obtained from $HAuCl_4$ by using PVP with molecular weights of 10, 40, and 360 K, respectively, are compared. There are significant changes in the shape, size, and color of the product materials. When a short chain PVP (10 K) is used, small spherical nanoparticles with average diameters of 8 nm are produced. On the other hand, triangular and hexagonal nanoplates

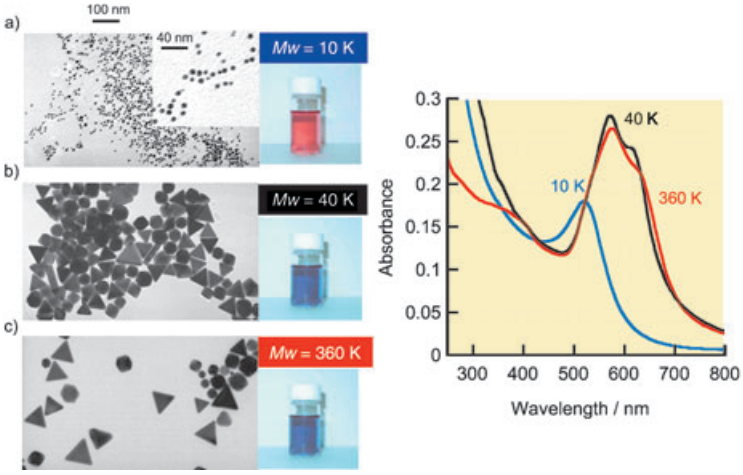

Figure 5. TEM photographs of Au nanostructures, color, and UV-visible spectra obtained from $HAuCl_4 \cdot 4H_2O$/PVP/EG by CW MW heating for 2 min with PVP molecular weights of a) 10 K, b) 40 K, and c) 360 K. Concentrations of $HAuCl_4 \cdot 4H_2O$ and PVP were the same as those in Figure 3.

with average edge lengths of 65 and 80 nm are formed by using PVP (40 K) and PVP (360 K), respectively. The color of the solution changes from wine red to blue on going from PVP with a molecular weight of 10 K to PVP with a molecular weight of 40 or 360 K. This color change is reflected by the shifts observed in the UV-visible absorption spectra. The visible absorption spectrum obtained with 10 K PVP exhibits a typical surface-plasmon band due to spherical nanoparticles in the 500–600 nm region with a sharp peak at about 520 nm.[8,35] On the other hand, broader surface-plasmon bands of Au appear in the 500–800 nm region with a peak at about 580 nm in the presence of 40 and 360 K PVP. A comparison between the UV-visible absorption spectra and TEM suggests that the longer wavelength component in the 550–800 nm region arises from surface-plasmon bands of polygonal Au nanoplates. As shown in the case of Ag nanostructures, UV-visible absorption spectra are useful to characterize product structures from the analysis of surface-plasmon resonance bands.[36]

Effects of solvent: Water has a large dielectric loss factor, though it has little reduction ability with respect to metallic salts. Au nanostructures were prepared by using water as a solvent. Although no reduction occurred without adding PVP, Au nanostructures could be synthesized by premixing PVP with $HAuCl_4$. This suggests that PVP can reduce metallic salts in water. Figure 6 shows TEM photographs of Au nanostructures obtained from $HAuCl_4$/PVP/H_2O solutions by using PVP (10, 40, and 360 K), respectively. Small spherical nanoparticles, and square and triangular nanoplates with diameters or edge lengths of 2–20 nm were produced by using a short chain PVP (10 K). SAED patterns of small spherical nanoparticles gave ring structure, as shown in the inset of Figure 6a, indicating that these nanoparticles are polycrystalline. When longer chain PVPs (40, 360 K,) were used, besides small spherical nanoparticles with diameters of 100–400 nm, large triangular, truncated triangular, and hexagonal plates with edge lengths of 0.3–1.5 μm were preferentially formed. SAED patterns of these polygonal plates exhibited similar hexagonal patterns to that shown in Figure 3a. It was therefore concluded that large triangular, truncated triangular, and hexagonal nanoplates are single-crystalline Au nanoplates. Based on the above results, a combination of slow reduction at a low temperature and a long-chain PVP is effective for the preparation of large Au triangular and hexagonal plates by the MW–polyol method. As shown above, the concentration of reagent and surfactant, the chain length of surfactant polymer, and the solvent are useful experimental parameters for the control of morphologies and sizes of Au nanostructures.

Preparation of Au nanorods and nanowires: In addition to spherical nanoparticles and nanoplates, small amounts of rods and wires were produced. Figure 7 shows Au rods and wires prepared under different $HAuCl_4$ concentrations at a constant PVP/$HAuCl_4$ molar ratio of 110. It is clear that diameters and lengths of rods and wires increase with increas-

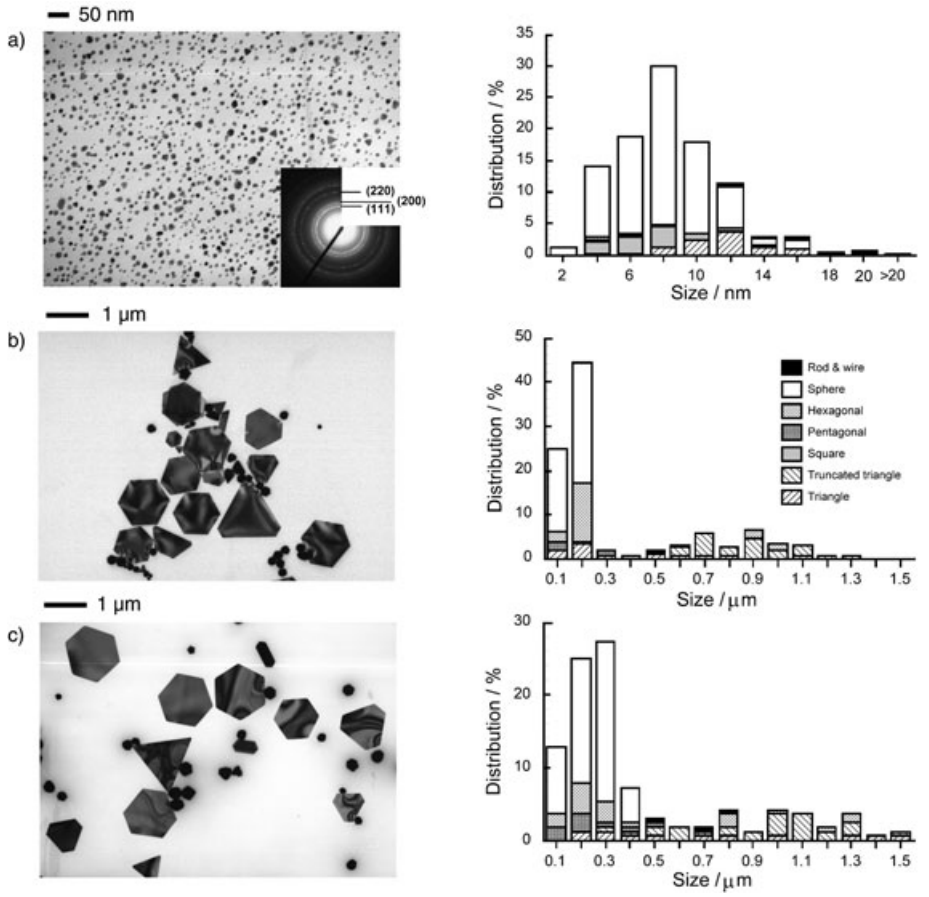

Figure 6. TEM photographs of Au nanostructures obtained by CW MW heating for 4 min from $HAuCl_4 \cdot 4H_2O$/PVP/H_2O with PVP molecular weights of a) 10 K, b) 40 K, and c) 360 K. Concentrations of $HAuCl_4 \cdot 4H_2O$ and PVP were 2.4 mM and 1.0 M, respectively.

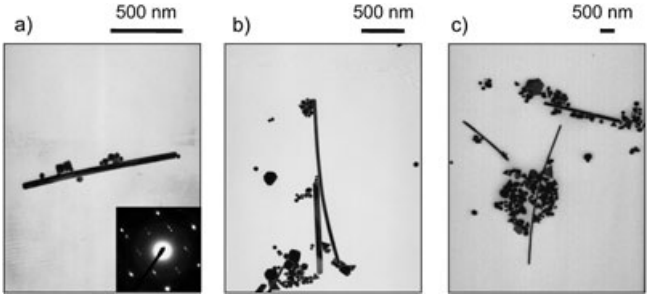

Figure 7. TEM photographs of Au nanorods and nanowires obtained from $HAuCl_4 \cdot 4H_2O$/PVP/EG by CW MW heating for 2 min in the presence of PVP (40 K). $HAuCl_4 \cdot 4H_2O$ and PVP concentrations were a) 2.4 mM and 0.264 M, b) 9.6 mM and 1.06 M, and c) 19.2 mM and 2.11 M, respectively (reprinted from reference [21] copyright (2004), with permission from Elsevier).

ing the $HAuCl_4$ concentration; this is also consistent with the size change of polygonal plates for the $HAuCl_4$ concentration. The total distribution of nanorods and nanowires is 2–16%, independent of $HAuCl_4$ and PVP concentrations. On the other hand, the average lengths of rods and wires increase from 50 to 350 nm with increasing $HAuCl_4$ concentration and decreasing PVP concentration. The SAED pattern of rods and wires indicated that Au rods and wires tend to growth as bicrystals twined along the {111} planes.

Zhu and Hu[14] have recently synthesized Au nanorods and nanowires by reducing $HAuCl_4$ in EG in the presence of PVP/sodium dodecyl sulfate at 160 °C. Liu et al.[19] synthesized Au nanorods in an aqueous solution in the presence of the tetradecylammoniumbromide (TOAB) cation as a surfactant. They found that Au nanorods with a higher aspect ratio could be produced at higher TOAB concentration and faster rising reaction temperature. With increasing TOAB concentration, the percentage of nanorods increased from 6 to 29.5%. On the basis of these findings, Au nanorods and nanowires could be synthesized under MW heating by using appropriate surfactants that induce anisotropic growth.

Formation mechanism of Au nanostructures: Anisotropic Au polygonal plates, rods, and wires could be synthesized efficiently under MW heating owing to various thermal and nonthermal effects described above. Although the detailed mechanism for the formation of each Au nanostructure under MW heating conditions is still uncertain, the following general mechanism can be proposed.

When EG was used, metallic particles (M) are produced from the following reactions according to reduction mechanism proposed by Fievet et al. [Eq. (2)].[1]

$$CH_2OH{-}CH_2OH \rightarrow CH_3CHO + H_2O \quad (2a)$$

$$2n\,CH_3CHO + 2\,M^{n+} \rightarrow 2\,M + 2n\,H^+ + n\,CH_3COCOCH_3 \quad (2b)$$

PVP acts as a capping reagent. The formation of anisotropic Au nanostructures is probably initiated by a reduction process [Eq. (2b)], leading to Au atoms that assemble to form the Au microcrystal particle. PVP that contains an N–C=O group is easily attached to the surface of these microcrystal and slows down the growth speed of the crystal facets. Different facets of this microcrystal have different adsorption ability. The facets that have fewer attached surfac-

tant moleculess grow more rapidly than those with more. As a result, they tend to assemble one by one to fabricate a specific shape. In this situation, PVP tends to attach to the lowest energy {111} facet and suppress the growth rate of this facet. Thus, anisotropic polygonal plates covered by {111} facets are preferentially produced.

In addition to polygonal plates, Au rods and wires are produced. As a result of reduction process [Eq. (2b)], Au metal, most of which is face-centered cubic (fcc), tends to nucleate and grow into twinned and multiply twinned particles with their surfaces bound by the lowest energy nucleation {111} facets. The surface energies of large particles are lower than those of smaller ones. It is therefore expected that some small nanoparticles are dissolved, while larger particles are grown to larger ones by means of an Ostwald ripening process.[37] With the assistance of PVP, some of the twinned particles grew into anisotropic rod-shaped and wire structures. For the Au/PVP system, we suspect that PVP might interact more strongly with the {100} facets (i.e., the side surfaces of Au rod and wire) than with the {111} facets (i.e., the ends of Au rod and wire). Once the rod-shaped structure has been formed, it can readily grow into a longer nanowire, because its side surfaces are tightly passivated by PVP and its ends are largely uncovered and remain reactive toward new Au atoms.

The PVP/$HAuCl_4$ molar ratio plays an important role in determining the morphologies of final products. A heavy coverage of PVP on the surfaces of nanoplates and nanoparticles results in an isotropic growth for all different faces leading to small nanostructures. With decreasing the coverage of PVP on the surfaces, the chance for the formation of anisotropic rod and wire structures increases. A decrease in coverage not only for the fast-growing end faces, but also for the side surfaces of each nanowire occurs at low PVP/$HAuCl_4$ ratios. Thus, thicker and longer nanowires are generally grown at low PVP/$HAuCl_4$ ratios.

Although definite adsorption and desorption mechanisms of PVP on the Au nanostructure formed under MW heating are uncertain, a possible reason for the formation of smaller nanoparticles with short chain PVP is a smaller adsorption volume, as shown in Scheme 2. Nonthermal effects, such as local heating of Au surfaces due to adsorption of long chain PVP, probably contributes to the formation of large anisotropic structures.

In the oil-bath heating, besides small amounts of short nanorods with aspect ratios below five and nanoplates, large spherical particles ($>$ 100 nm) were dominantly produced. No evidence for the formation of nanowires was observed in the oil-bath heating. Particles and plates in the oil-bath heating had less sharp edges than those formed under CW MW heating due to lower crystallization. Higher crystallization leading to single-crystalline Au nanoplates, nanorods, and nanowires under MW heating must be induced by bursting nucleation due to rapid and homogeneous MW heating.

Liu et al.[19] reported the formation mechanism of Au nanorods in the presence of the surfactant TOAB. In the presence of TOAB, the surface tension of solution is reduced; therefore, the energy needed to form a new phase becomes low. TOAB can also be considered to influence of the growth process of nanoparticles by the electrostatic and the stereochemical phenomena. TOAB is a positively charged tetrahedral compound with a long hydrophobic tail. The growth unit of Au is negatively charged. Ion pairs between TOA^+ and $AuCl_4^-$ can form due to electrostatic interaction. When the reduction process begins, rods start to form. In the crystallization process, TOAB may serve as a growth controller, as well as an agglomeration inhibitor by forming a covering film on the newly formed Au nanorods.[38] The above processes were enhanced under MW heating due to thermal and nonthermal effects.

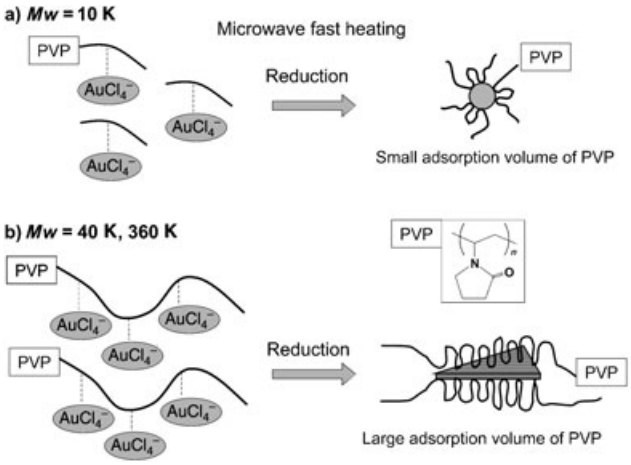

Scheme 2. Formation scheme of Au nanostructures by using PVP with different chain lengths.

Synthesis of Silver Nanostructures

The MW heating method has been used for the syntheses of Ag nanostructures.[8–11,16,17,20,22,23] In addition to Ag spherical nanoparticles, triangular plates, sheets, rods, wires, tubes, and dendrites have been prepared under MW irradiation.

Preparation of Ag spherical nanoparticles: Although Ag nanoparticles have been prepared by various methods, an ideal method for chemical preparation of size-controlled Ag nanoparticles is a chemical reduction with $NaBH_4$, resulting in the dodecanethiol-capped 1.8–3.5 nm diameter Ag nanoparticles. A disadvantage of this method is that size-selective precipitation is necessary. Yamamoto et al.[16] prepared Ag nanoparticles by alcohol reduction of fatty acid Ag salts suspended in 1-hexanol under MW irradiation for 1–5 min at 140–157 °C. They succeeded in the fast preparation of size-controlled Ag nanoparticles in the range 4.9–7.4 nm only by changing length of the alkyl chains in the fatty acids, as shown in Scheme 3.

Preparation of Ag triangular nanoplates (prism): He et al.[10] studied preparation of polygonal Ag nanoplates under MW

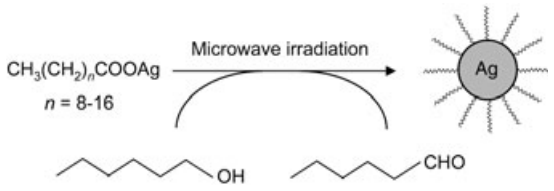

Scheme 3. Microwave–alcohol reduction of fatty acid Ag salts for the preparation of size-controlled Ag nanoparticles.

irradiation of $AgNO_3$ in the presence of PVP without any other reducing agent. They used four solvents, DMF (b.p. = 153 °C), NMP (b.p. = 202 °C), pyridine (115 °C), and ethanol (b.p. = 78 °C). They found that solvents have significant influence on the morphology of the Ag particles and on the color of solutions under MW irradiation, and that higher boiling point solvents were advantageous to the higher crystallinity of the Ag nanopartilces. When DMF, which has a good reducing ability and a high boiling point, was used, triangular (edge length = 50–100 nm) or truncated triangular nanoprisms were preferentially formed, while nanoprisms with lower regularity were produced in NMP. On the other hand, monodispersed spherical particles with an average diameter of 8 and 32 nm were obtained in pyridine and ethanol, respectively, which have low boiling points.

Yamamoto et al.[23] prepared triangular Ag nanoplates by using MW-promoted reduction of $AgNO_3$ in aqueous solutions in the presence PVP (40 K). As shown in the upper part of Scheme 4, only spherical Ag nanoparticles were prepared at a low $AgNO_3$ concentration of 0.01 M. When the concentration of $AgNO_3$ was increased to 0.1 M, spherical Ag particles were converted to prisms with increasing the MW irradiation time, but no small prismatic nuclei were found, even at the initial stage of crystallization (lower part of Scheme 4). The triangular Ag nanoplates should be formed by a shape-transformation from a sphere to a prism

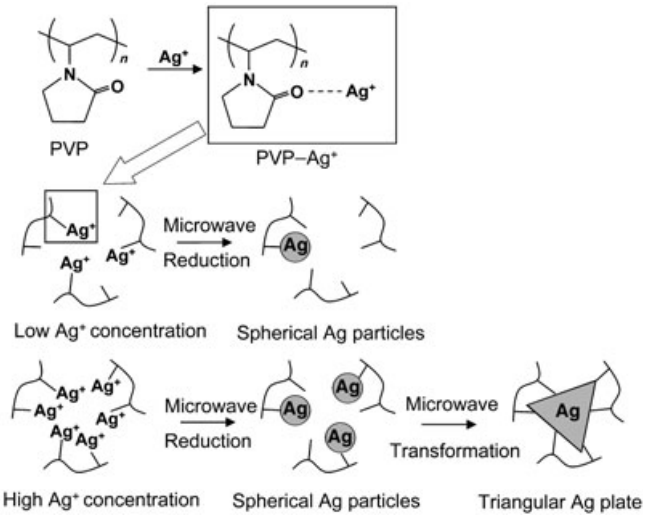

Scheme 4. Preparation of triangular Ag nanoplates under MW microwave heating of $AgNO_3$/PVP in an aqueous solution.

during the crystal-growth process under MW irradiation. They concluded that MW irradiation should accelerate the coherent heating of PVP-stabilized silver surfaces, resulting in a shape transformation from spherical silver particles to the large silver prism in the prolonged MW-promoted heating system, in which a reconstruction of the crystallites may occur, for example, through Ostwald ripening.[37]

Preparation of Ag nanorods, nanowires, nanosheets, and nanotubes: We have succeeded in the large-scale synthesis of Ag nanorods and nanowires from $AgNO_3/H_2PtCl_6$/PVP(40 K)/EG under MW heating.[17,22] When a mixture of $AgNO_3$/PVP/EG was irradiated for 3–8 min without adding H_2PtCl_6, only uniform spherical Ag nanoparticles with diameters of ~80 nm are observed in TEM photographs (Figure 8a). By premixing a small amount of H_2PtCl_6 with the $AgNO_3$/PVP/EG mixture as a source of Pt seeds, Ag nanorods and nanowires could be prepared. We found that the morphology and aspect ratios of the Ag nanorods and nanowires strongly depended on the experimental parameters especially the PVP/$AgNO_3$ molar ratio at a constant $AgNO_3$ concentration, and $AgNO_3$ and PVP concentrations at a constant PVP/$AgNO_3$ molar ratio. Ag nanostructures were synthesized at PVP/$AgNO_3$ ratios from 0.5 to 24. In addition to spherical nanoparticles, anisotropic nanorods and nanowires are produced at all PVP/$AgNO_3$ molar ratios investi-

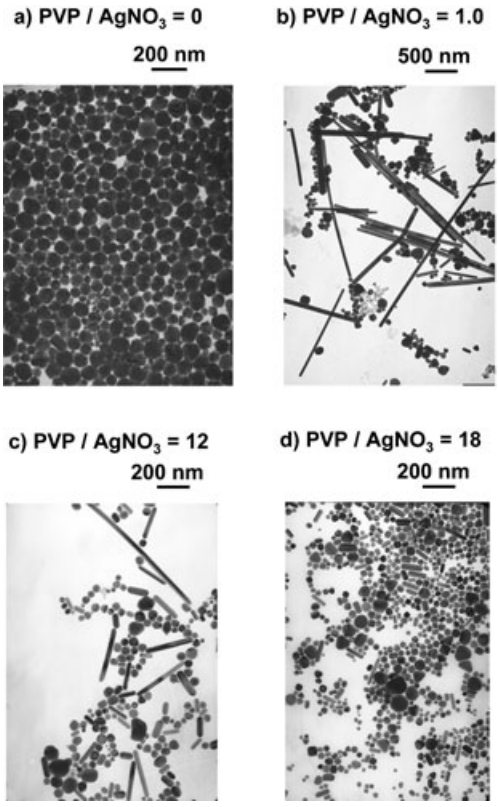

Figure 8. TEM photographs of Ag nanostructures prepared by MW heating for a) $AgNO_3$/PVP(40 K)/EG and b)–d) $AgNO_3/H_2PtCl_6$/PVP(40 K)/EG. Concentrations of $H_2PtCl_6 \cdot 6H_2O$ and $AgNO_3$ were kept at 5.78 μM and 23.1 mM, respectively.

gated, as shown in Figure 8b–d for PVP/$AgNO_3$ molar ratios of 1.0, 12, and 18, respectively. The diameters and lengths of nanorods and nanowires were 30–140 nm and 0.3–10 μm, respectively. In general, diameters of spherical nanoparticles and aspect ratios of rods and wires decrease with increasing PVP/$AgNO_3$ molar ratio, and only short nanorods are produced at high PVP/$AgNO_3$ molar ratio range of 18–24. The fractions of nanonods and nanowires at a constant PVP/$AgNO_3$ molar ratio of 5.7 increased with increasing the $AgNO_3$ concentration, and their fractions were about 80% at a high $AgNO_3$ concentration of 92 mM. The aspect ratios of rods and wires increased with increasing the $AgNO_3$ concentration. These findings imply that low PVP/$AgNO_3$ ratios and high $AgNO_3$ and PVP concentrations are required for the synthesis of long wires with large diameters. Although similar nanorods and nanowires have been synthesized by conventional oil-bath heating from similar solutions,[39] it took more than 50 min to prepare long nanowires. The advantage of MW heating is that similar long nanowires could be synthesized within a few minutes under the optimum conditions.

Figure 9a–d shows TEM photographs after MW irradiation for 1.5 and 3 min at PVP/$AgNO_3$ molar ratios of 2.0 and 3.0. It should be noted that various shapes and sizes of Ag nanosheets are synthesized at these short irradiation times. These nanosheets disappeared under MW irradiation above 5 min. The fraction of anisotropic nanosheets in the products was large at low PVP/$AgNO_3$ molar ratio range of 0.5–3.0, as in the cases of rods and wires. To the best of our knowledge, no Ag nanosheets have been prepared in oil-bath heating.

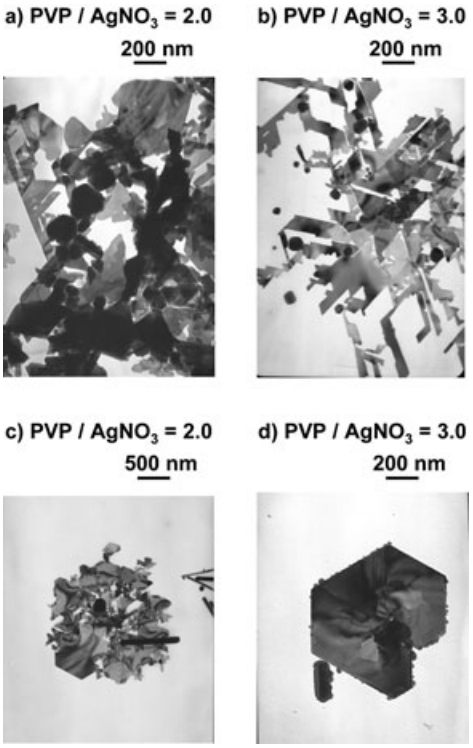

Figure 9. TEM photographs of Ag nanosheets obtained from $AgNO_3$/$H_2PtCl_6{\cdot}6H_2O$/PVP(40 K)/EG by CW MW heating for a,b) 1.5 min and c,d) 3 min.

SAED patterns of wires and sheets were measured. Typical results obtained for a wire and a sheet are shown in Figure 10 (left and right, respectively). These SAED patterns indicate that the Pt seeds are fully enveloped in Ag nanostructures. Based on SAED patterns, Ag rod and wires tend to growth as bicrystals twined along the {111} planes for fcc Ag crystals. Hexagonal patterns and the interval of each array of the sheets led us to conclude that Ag sheets are composed of single-crystalline Ag and the incident electron beams are perpendicular to {111} facets of the nanosheets.

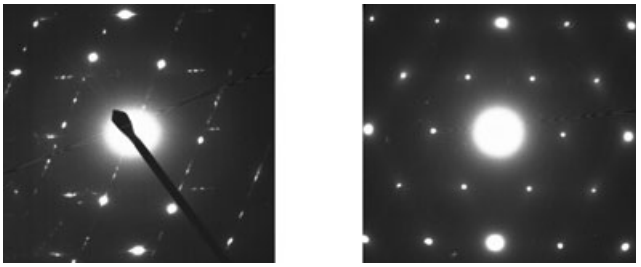

Figure 10. SAED patterns of an Ag nanowire (left) and an Ag nanosheet (right).

The formation of anisotropic Ag nanostructures is initiated by reducing H_2PtCl_6 in EG [Eq. (3)].

$$4\,CH_3CHO + Pt^{4+} \rightarrow Pt + 4\,H^+ + 2\,CH_3COCOCH_3 \qquad (3)$$

As a result of the above reduction process, very small Pt nanoparticles are initially formed as seeds. A similar reduction process occurs for $AgNO_3$ as a competitive process [Eq. (4)].

$$2\,CH_3CHO + 2\,Ag^+ \rightarrow 2\,Ag + 2\,H^+ + CH_3COCOCH_3 \qquad (4)$$

We found that nanorods and nanowires were not produced without adding H_2PtCl_6. This indicates that Pt seeds play an important role in determining the morphologies of the final products. The exact mechanism for the formation of the different morphologies of the Ag particles in the presence of H_2PtCl_6 under MW irradiation is still unclear. The following two reasons are proposed by El-Sayed et al.[40] for the formation of anisotropic rodlike particles: 1) the growth rates vary at different planes of the particles and 2) particle growth competes with the coordinating action of stabilizers. When $AgNO_3$ was reduced by EG with the assistance of Pt seeds and PVP, the initial product was a mixture of Ag nanoparticles and small quantity of nanorods.[22] The formation mechanism is probably due to fact that PVP kinetically controls the growth rates of various faces by the different rates of reduction of coordinated and uncoordinated Ag^+ ions at sites on the Pt seeds and their different rates of diffu-

sion at these sites on the seeds. Under reduction of Ag^+ by MW heating, some Ag nanostructures started to dissolve into the solution and grow into Ag nanoparticles and nanorods through an Ostwald ripening process.[37] A heavy coverage of PVP on the surfaces of nanoparticles results in small spherical nanoparticles. With decreasing the coverage of PVP on the surfaces, the fraction of anisotropic rod and wire structures increases. In general, thicker and longer Ag nanorods and nanowires are grown at low $PVP/AgNO_3$ ratios at a constant $AgNO_3$ concentration, and high $AgNO_3$ and PVP concentrations at a constant $PVP/AgNO_3$ ratio.

Zhu and Hu[20] reported that the MW-assisted polythiol reduction (MPTR) method, with 1,2-ethanedithiol (EDT) as both a reducing reagent and a solvent, is useful for fast preparation of Ag nanowires from Ag_2O solid by means of a solid–liquid reaction mechanism at temperatures between 80 and 140 °C. In addition to single-crystalline Ag nanowires (Figure 11a and b), tubelike structures with a diameter of 290 nm and a length of 3 mm were observed in a few cases (Figure 11c and d). The tube was partially filled with nanoparticles in the case of Figure 11d. The diameter of tubelike structures was uniform and the structures were amorphous, as indicated by the ED pattern shown in the inset of Figure 11d. It should be noted that twinned rods were also observed as a minor product (Figure 11e). Each twinned rod consisted of two parallel rods that grew together, one rod with a diameter of 110 nm and the other 160 nm, both with a length of 2.2 mm. Other twinned rods with various diameters and lengths were also observed.

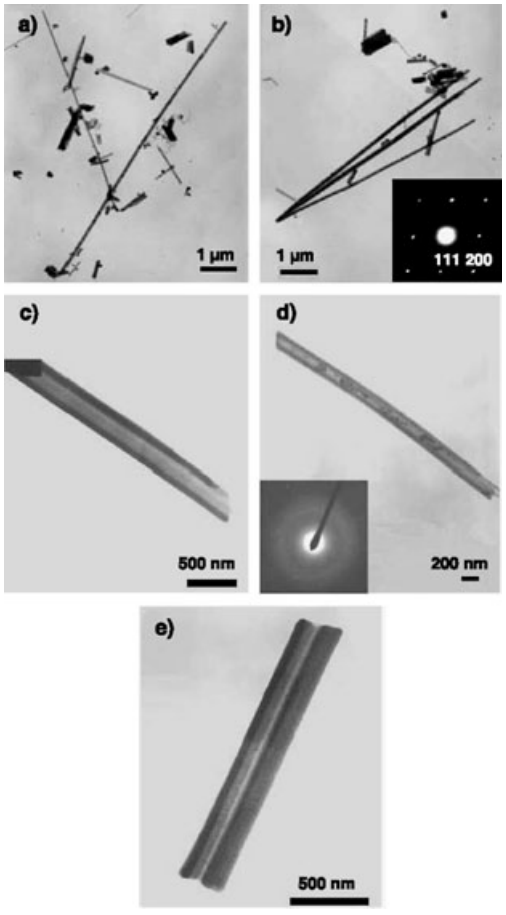

Figure 11. TEM micrographs of Ag nanostructures prepared by the MPTR method (a,b). The inset of b) shows the ED pattern of a single nanowire. c,d,e) Ag nanotubes (reprinted from reference [20] copyright (2004), with permission from Elsevier).

They also prepared Ag nanostructures by the MW-assisted polyol method for comparison. Their experiments showed that Ag products prepared by heating Ag_2O in EG by MW irradiation at temperatures between 80 and 190 °C consisted of only spherical particles. No Ag nanowires or nanorods were observed in all these samples. Therefore, the MPTR method is favorable for production of Ag nanowires. Although the detailed mechanism for the formation of Ag nanowires by using a dithiol solvent under MW heating is unclear, the solvent and reducing reagent greatly influence the morphology of Ag nanostructures prepared from solid–liquid reactions. An outstanding feature of the MPTR method is that surfactant is unnecessary for the preparation of Ag nanowires or nanorods from solid–liquid reactions.

Preparation of Ag dendrites: He et al.[11] prepared well-defined Ag dendrites by reduction of $AgNO_3$ in DMF in the presence of PVP (40 K) under MW irradiation, as shown in Figure 12. Morphology similar to that of the diffusion-limited aggregation model with fractal dimensions around 1.7 has been observed. MW power and the existence of PVP play important roles in the formation of well-defined Ag dendrites.

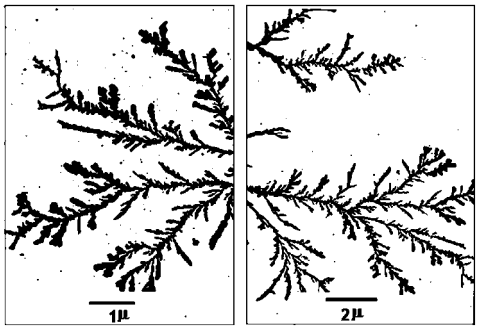

Figure 12. TEM images of the Ag dendrites prepared under MW heating. Large and bright fractals were formed. Reprinted from reference [11] copyright (2004), with permission from Elsevier.

According to their proposed mechanism for the formation of Ag dendrites, Ag ions were reduced by DMF and PVP under MW irradiation and some metallic Ag nanoparticles were formed at the beginning of the reaction. As the reaction progressed, the interaction between Ag particles and MW energy may lead to a rise in temperature in surrounding regions and may stimulate new nuclei to appear at its boundary for further diffusion-limited growth. Therefore, the rate of the nucleation and growth of the crystal controlled the formation of the dendrites. PVP can kinetically con-

trol the growth rates of various faces of Ag crystals by interacting with these faces through adsorption and desorption. The faceted growth of Ag crystal under MW irradiation induced the formation of the anisotropic silver nanoparticles capped by PVP. The formation of the dendritic fractal structure associated with the anisotropic morphology of the Ag particles under MW irradiation. They reported that the dendrites were genuine structures obtained under MW irradiation.

Preparation of Bimetallic Nanoparticles

Bimetallic particles have received considerable attention, because of their superior catalytic properties to those of monometallic nanoparticles and the change in their surface-plasmon band energy relative to that of the separate metals. Recently the MW–polyol method has been applied to the preparation of bimetallic nanopartilces. In general, the solution reactions for the formation of binary chalcogenides are relatively slow and are conducted under hydro-or solvothermal conditions in special high-temperature and high-pressure equipment in order to accelerate their rate. Even under these conditions the reaction takes many hours or even days. Recently, Harpness and Gedanken[31] succeeded in the preparation of binary chalcogenides (selenides and tellurides) and core-shell gold/palladium bimetallic nanoparticles by the simultaneous reduction of the Au^{3+} and Pd^{2+} ions in EG under MW heating. In most experiments, the MW reaction was completed within a few minutes, the maximum duration being 1 h.

Figure 13 shows a high-resolution TEM image of Au/Pd core-shell structure. Thermodynamically, it is easier to reduce the Au ions, because the reduction potential of Au is more positive than that of Pd. However, it was not known from early studies whether the reduction of the $AuCl_4^-$ ions was faster than that of the $PdCl_4^{2-}$ ions. Their results gave the answer to this dilemma and indicated that Au is reduced first forming the particle's core followed by the reduction of palladium. The Au^0 acts as a nucleic center for the growth of the Pd layer, which covers Au and grows to its final size.

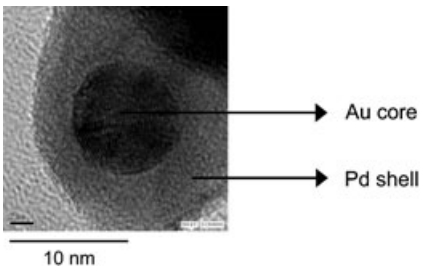

Figure 13. High-resolution TEM image of core-shell Au/Pd prepared by MW heating for 1 h under N_2 (reprinted from reference [31] copyright (2004), with permission from the American Chemical Society).

Preparation of Nanoparticles on Carbon Nanomaterials

Pt nanoparticles supported on Vulcan XC-72 carbon black (CB), carbon nanotubes (CNT), and carbon nanofibers (CNF) were prepared by a MW-assisted polyol process.[29,30,41] Figure 14a and b shows Pt nanoparticles prepared on carbon black and on herringbone-type carbon nanofibers in EG.[41] It is seen that well-dispersed Pt nanoparticles with 2–10 nm in diameter are prepared on these carbon nanomaterials. Similar well-dispersed PtRu nanoparticles with diameters in the range 2–6 nm on CB and CNT have been prepared by Liu et al.[30] They found that both PtRu/C catalysts had high and more durable electrocatalytic activities for methanol oxidation than a comparable Pt/C catalyst. These data indicate that the MW–polyol method is a promising way to synthesize nanoparticles supported on carbon materials for fuel cells. One reason for the synthesis of well-dispersed nanoparticles on carbon under MW heating is that carbon is a good MW absorber. Therefore, hot spots, which accelerate reduction and nucleation of metals, are created on the surfaces of carbon supports.

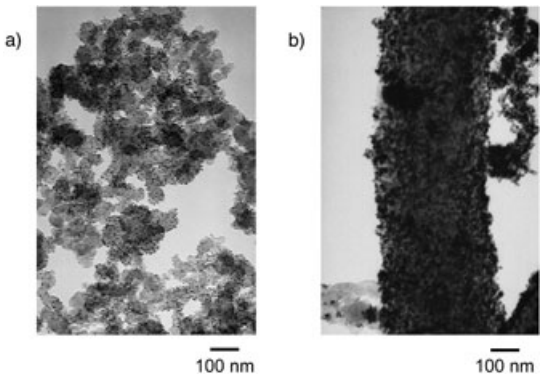

Figure 14. TEM photographs of Pt deposited on a) carbon black and b) herringbone-type carbon nanofibers prepared by MW heating in EG for 2 min.

Conclusion

The advantages of MW dielectric heating for the synthesis of metallic nanostructures have been demonstrated by using some selected examples. The main advantages of MW irradiation are 1) uniform heating of the solution, so that a more homogeneous nucleation is obtained as well as a shorter crystallization time; 2) very short thermal induction period, which can lead to energy savings; 3) generation of localized high temperatures at the reaction sites which results in enhancement of reduction rates of metallic ions; 4) selective formation of specific morphology; and 5) superheating of solvents over the boiling points of solvent as a consequence of the microwave dissipation over the whole liquid volume.

Further advantages are absence of convection processes, easy control, and low cost. Due to these advantages, monodispersed and better crystalline metallic nanostructures could be synthesized in a one-pot reaction within a few minutes. Since MW heating is a promising heating method, a further wide application to preparation and control of various kinds of metallic nanostructures, which are key materials in nanotechnology, is expected. Unfortunately, detailed mechanism for the preparation of metallic nanostructures under MW irradiation has not been clarified. In order to clarify thermal and nonthermal effects of MW irradiation in each reaction system, further detailed experimental studies and model calculations will be necessary.

Acknowledgement

This work was partially supported by a Grant-in-Aid for Scientific Research No. 15651046 from the Japanese Ministry of Education, Culture, Sports, Science, and Technology. We thank Profs. I. Mochida and S.H. Yoon of our Institute for supplying us with herringbone-type carbon nanofibers and the Research Laboratory for High Voltage Electron Microscopy, Kyushu University for the use of TEM.

[1] F. Fievet, J. P. Lagier, B. Blin, B. Beaudoin, M. Fiflarz, *Solid State Ionics* **1989**, *32/33*, 198.
[2] a) P.-Y. Silvert, R. Herrera-Urbina; N. Duvauchelle, V. Vijayakrishnan, K. Tekaia-Elhsissen, *J. Mater. Chem.* **1996**, *6*, 573; b) P.-Y. Silvert, R. Herrera-Urbina, K. Tekaia-Elhsissen, *J. Mater. Chem.* **1997**, *7*, 293.
[3] M. S. Hedge, D. Larcher, L. Dupont, B. Beaudoin, K. Tekaia-Elhsissen, J. M. Tarascon, *Solid State Ionics* **1997**, *93*, 33.
[4] Y. Wada, H. Kuramoto, T. Sakata, H. Mori, T. Sumida, T. Kitamura, S. Yanagida, *Chem. Lett.* **1999**, *28*, 607.
[5] W. Tu, H. Liu, *J. Mater. Chem.* **2000**, *10*, 2207.
[6] Z. L. Jiang, Z. W. Feng, X. C. Shen, *Chin. Chem. Lett.* **2001**, *12*, 551.
[7] M. Tsuji, M. Hashimoto, T. Tsuji, *Chem. Lett.* **2002**, *31*, 1232.
[8] I. Pastoriza-Santos, L. Liz-Marzán, *Langmuir* **2002**, *18*, 2888.
[9] S. Komarneni, D. Li, B. Newalkar, H. Katsuki, A. S. Bhalla, *Langmuir* **2002**, *18*, 5959.
[10] R. He, X. Qian, J. Yin, Z. Zhu, *J. Mater. Chem.* **2002**, *12*, 3783.
[11] R. He, X. Qian, J. Yin, Z. Zhu, *Chem. Phys. Lett.* **2003**, *369*, 454.
[12] F. K. Liu, C. J. Ker, Y. C. Chang, F. H. Ko, T. C. Chu, B. T. Dai, *Jpn. J. Appl. Phys. Part 1* **2003**, *42*, 4152.
[13] M. Tsuji, M. Hashimoto, Y. Nishizawa, T. Tsuji, *Chem. Lett.* **2003**, *32*, 1114.
[14] Y. J. Zhu, X. L. Hu, *Chem. Lett.* **2003**, *32*, 1140.
[15] R. Harpeness, A. Gedanken, A. M. Weiss, M. A. Slifkin, *J. Mater. Chem.* **2003**, *13*, 2603.
[16] T. Yamamoto, Y. Wada, T. Sakata, H. Mori, M. Goto, S. Hibino, S. Yanagida, *Chem. Lett.* **2004**, *33*, 158.
[17] M. Tsuji, Y. Nishizawa, M. Hashimoto, T. Tsuji, *Chem. Lett.* **2004**, *33*, 370.
[18] W. X. Chen, J. Zhao, J. Y. Lee, Z. L. Liu, *Chem. Lett.* **2004**, *33*, 474.
[19] F. Liu, Y. Chang, F. Ko, and T. Chu, *Mater. Lett.* **2004**, *58*, 373.
[20] Y. J. Zhu, X. L. Hu, *Mater. Lett.* **2004**, *58*, 1517.
[21] M. Tsuji, M. Hashimoto, Y. Nishizawa, T. Tsuji, *Mater. Lett.* **2004**, *58*, 2326.
[22] M. Tsuji, M. Hashimoto, Y. Nishizawa, T. Tsuji, *Hoshasen Kagaku (Radiation Chem.)* **2004**, *77*, 8, in Japanese.
[23] T. Yamamoto, H. Yin, Y. Wada, T. Kitamura, T. Sakata, H. Mori, S. Yanagida, *Bull. Chem. Soc. Jpn.* **2004**, *77*, 757.
[24] O. Palchik, R. Kerner, A. Gedanken, A. M. Weiss, M. A. Slifkin, V. Palchik, *J. Mater. Chem.* **2001**, *11*, 874.
[25] Y. Wada, H. Kuramoto, J. Anand, T. Kitamura, T. Sakata, H. Mori, S. Yanagida, *J. Mater. Chem.* **2001**, *11*, 1936.
[26] T. Yamamoto, Y. Wada, H. Yin, T. Sakata, H. Mori, S. Yanagida, *Chem. Lett.* **2002**, *31*, 964.
[27] T. Ding, J. Zhang, S. Long, J. Zhu, *Microelectron. Eng.* **2003**, *66*, 46.
[28] H. Grisaru, O. Palchik, A. Gedanken, V. Palchik, M. A. Slifkin, A. M. Weiss, *Inorg. Chem.* **2003**, *42*, 7148.
[29] Z. L. Liu, X. Y. Ling, J. Y. Lee, X. D. Su, L. M. Gan, *J. Mater. Chem.* **2003**, *13*, 3049.
[30] Z. L. Liu, J. Y. Lee, W. X. Chen, M. Han, L. M. Gan, *Lamgmuir* **2004**, *20*, 181.
[31] R. Harpeness, A. Gedanken, *Langmuir* **2004**, *20*, 3431.
[32] *Microwave-Enhanced Chemistry: Fundamentals, Sample Preparation, Applications* (Eds.: H. M. Kingston, S. J. Haswell), American Chemical Society, Washington DC, **1997**.
[33] S. A. Galema, *Chem. Soc. Rev.* **1997**, *26*, 233.
[34] Y. Sun, Y. Xia, *Science* **2002**, *298*, 2176.
[35] A. Henglein, *Langmuir* **1999**, *15*, 6738.
[36] J. A. Creighton, D. G. Eadon, *J. Chem. Soc. Faraday Trans.* **1991**, *87*, 3881.
[37] A. R. Roosen, W. C. Carter, *J. Phys. A* **1998**, *261*, 232.
[38] X. M. Sun, X. Chen, Z. X . Deng, Y. D. Li, *Mater. Chem. Phys.* **2002**, *78*, 99.
[39] Y. Sun, Y. Yin, B. Mayers, T. Herricks, Y. Xia, *Chem. Mater.* **2002**, *14*, 4736.
[40] J. M. Petroski, Z. L. Wang, T. C. Green, M. A. El-Sayed, *J. Phys. Chem. B* **1998**, *102*, 3316.
[41] M. Tsuji, M. Kubokawa, K. Matsumoto, Y. Nishizawa, T. Tsuji, S. H. Yoon, I. Mochida, unpublished results.

Published online: October 29, 2004